Available online at www.sciencedirect.com
SCIENCE DIRECT®
International Journal of Heat and Mass Transfer 48 (2005) 3443–3453
International Journal of HEAT and MASS TRANSFER
www.elsevier.com/locate/ijhmt

MHD natural convection in a laterally and volumetrically heated square cavity

I.E. Sarris, S.C. Kakarantzas, A.P. Grecos, N.S. Vlachos *

Laboratory of Fluid Mechanics and Turbomachines, Department of Mechanical and Industrial Engineering, University of Thessaly, 38334 Volos, Greece

Received 28 July 2004

Abstract

A numerical study is presented of unsteady two-dimensional natural convection of an electrically conducting fluid in a laterally and volumetrically heated square cavity under the influence of a magnetic field. The flow is characterized by the external Rayleigh number, Ra_E, determined from the temperature difference of the side walls, the internal Rayleigh number, Ra_I, determined from the volumetric heat rate, and the Hartmann number, Ha, determined from the strength of the imposed magnetic field. Starting from given values of Ra_E and Ha, for which the flow has a steady unicellular pattern, and gradually increasing the ratio $S = Ra_I/Ra_E$, oscillatory convective flow may occur. The initial steady unicellular flow for $S = 0$ may undergo transition to steady or unsteady multicellular flow up to a threshold value, $Ra_{I,cr}$, of the internal Rayleigh number depending on Ha. Oscillatory multicellular flow fields were observed for S values up to 100 for the range 10^5–10^6 of Ra_E studied. The increase of the ratio S results usually in a transition from steady to unsteady flow but there have also been cases where the increase of S results in an inverse transition from unsteady to steady flow. Moreover, the usual damping effect of increasing Hartmann number is not found to be straightforward connected with the resulting flow patterns in the present flow configuration.

1. Introduction

The concept of liquid-metal breeder blanket for a fusion reactor [1,2] has motivated various studies of MHD flows, including natural convection. In modelling such a system, several factors should be taken into account, in particular the inhomogeneity of the (strong) external magnetic field and the three-dimensionality of the enclosure. Numerical simulations of buoyancy-driven flows in cubic enclosures subject to a static homogeneous magnetic field [3–5] have led to some interesting results. However, because of their simplicity and despite their limited physical significance, investigations of two-dimensional flows should are often considered. They permit to analyze in more detail the dependence of the flow when the parameters of the problem are varied in a relatively broad range. In the present work, the influence of a homogeneous magnetic field on the natural convection of a liquid-metal in a square cavity is being studied, assuming that the flow is affected both by a sidewall temperature difference and by internal heating.

The independent group of parameters that describe the present MHD cavity flow are the external Rayleigh number $Ra_E = g\beta\Delta TH^3/\nu\alpha$ due to the temperature difference ΔT $(=T_1 - T_2)$ of the sidewalls, the internal Rayleigh number $Ra_I = g\beta GH^5/\nu k\alpha$ due to volumetric

* Corresponding author.
E-mail address: vlachos@mie.uth.gr (N.S. Vlachos).

0017-9310/$ - see front matter © 2005 Elsevier Ltd. All rights reserved.
doi:10.1016/j.ijheatmasstransfer.2005.03.014

Nomenclature

B_0	magnitude of the external magnetic field
f	frequency
G	volumetric heating rate
g	gravitational acceleration
H	height of the cavity
Ha	Hartmann number ($= B_0 H\sqrt{\sigma/\rho\nu}$)
k	thermal conductivity
$\overline{Nu}$	average Nusselt number
p	fluid pressure
Pr	Prandtl number
Ra_E	external Rayleigh number ($=g\beta\Delta T H^3/\nu\alpha$)
Ra_I	internal Rayleigh number ($=g\beta G H^5/\nu k\alpha$)
S	Ra_I/Ra_E
ΔS	increment of increasing S
T	fluid temperature
ΔT	temperature difference of the side walls ($T_1 - T_2$)
t	time
Δt	time step
$\mathscr{T}$	period of an oscillation
u, v	velocity components in x and y directions
x, y	spatial coordinates

Greek symbols

α	thermal diffusivity
β	coefficient of thermal expansion
ν	fluid kinematic viscosity
ρ	fluid density
σ	electric conductivity
τ	non-dimensional time
Ψ	non-dimensional stream function

Subscripts

cr	critical
min	minimum
max	maximum
ref	reference
1, 2	indices for the hot (right) and cold (left) wall

heating G, the Hartmann number $Ha = B_0 H\sqrt{\sigma/\rho\nu}$ and the fluid Prandtl number $Pr = \nu/\alpha$. The imposed horizontal magnetic field is considered uniform with constant magnitude B_0, g is the acceleration due to gravity, β is the coefficient of thermal expansion, H is the side of the square cavity, ν is the kinematic viscosity, α is the thermal diffusivity, k is the thermal conductivity, σ is the electrical conductivity, and ρ is the density. The ratio $S = Ra_I/Ra_E$ that determines which thermal mechanism (internal heating or sidewall temperature difference) has more influence on the flow and heat transfer is another important parameter.

A limited number of numerical works [6–8] have been reported for the study of simultaneously laterally and volumetrically heated cavities. These studies, corresponding to higher Pr numbers than those of liquid-metals, showed no oscillatory flows even at very high Ra_E and Ra_I. In the vicinity of volumetric heat sources, Gelfgat et al. [9] showed that, the smaller the Pr the lower the critical value of Grashof number ($Gr = Ra/Pr$) required for the onset of oscillatory instability. Moreover, the flow stabilization effect (connected with the external magnetic field) for the oscillatory flow of a liquid-metal in a laterally heated rectangular cavity was studied by Gelfgat and Bar-Yoseph [10]. They were surprised to conclude that the single-cell flow could be destabilized inside thin Hartmann boundary layers even with increasing Ha. For the case of low Pr (0.0321) natural convection in a volumetrically heated square cavity, Arcidiacono et al. [11] showed that the spatially symmetrical flow broke into asymmetric steady-state flow for $Gr \approx 3\times 10^7$, while the asymmetric flow became time-periodic for $Gr \approx 5\times 10^7$. Chaotic motion was also predicted for $Gr \geqslant 10^8$.

In this study, two-dimensional unsteady simulations of MHD natural convection of a liquid-metal in a laterally and volumetrically heated square cavity were performed in order to determine the dependence of the flow on the internal-to-external heating ratio S as well as on the Hartmann number. The numerical calculations were conducted starting from the steady unicellular solution of a given external Rayleigh number with no heating ($Ra_I = 0$) and gradually increasing S until oscillatory motion occurred. For the case of $Ra_E = 10^5$, steady unicellular flow patterns occur for $Ha > 0$, while for the case of $Ra_E = 10^6$ unsteady unicellular patterns were found for $Ha < 38$. Thus, for the latter case, simulations were conducted for $Ha \geqslant 38$ in order to start from steady flow patterns. Numerical calculations were carried out starting from $S = 0$ and gradually increasing S up to the value of 100. Results were obtained up to the moderate value of $Ha = 22$ for the case of $Ra_E = 10^5$ and $Ha = 76$ for the case of $Ra_E = 10^6$. For higher Ha values, the flow remained steady for all the S values studied. The total number of unsteady simulations summarized in the present work is about 1500.

2. Mathematical formulation and numerical details

Consider the two-dimensional square cavity of Fig. 1 of side H filled with a liquid-metal. The right wall is maintained at a uniform constant temperature T_1, while the left at a lower temperature T_2. The liquid-metal

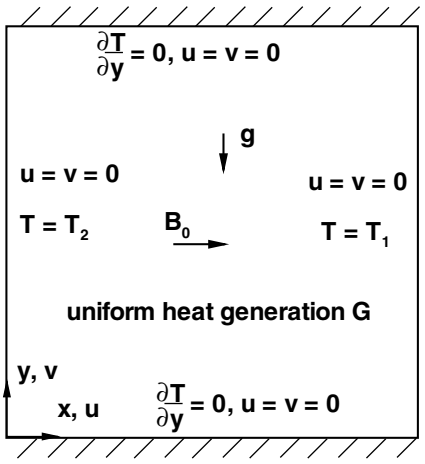

Fig. 1. Flow geometry and boundary conditions.

contained in the cavity is also subjected to a uniform internal volumetric heating of power G. The top and bottom walls are thermally insulated. The electrically conducting fluid interacts with an external horizontal uniform magnetic field of constant magnitude B_0. Assuming that the flow induced magnetic field is very small compared to B_0 (low-R_m approximation [12]) and considering electrically insulated cavity walls, the electromagnetic force can be reduced to the damping factor $-B_0^2 v$ [13], where v is the vertical velocity component. Thus, the Lorentz force depends only on the velocity component perpendicular to the magnetic field.

According to Ostrach [14], for highly convective flows of low-Pr number fluids like the liquid-metal considered here, the most suitable reference velocity is: $u_{ref} = (g\beta\Delta TH)^{1/2}$. Thus, the governing equations (continuity, momentum and energy) can be put into dimensionless form by scaling the length with the height H of the cavity, velocity with u_{ref}, pressure with ρu_{ref}^2, temperature with ΔT, magnetic induction with B_0, and time with H/u_{ref}. The dimensionless temperature is defined as $T = (T^* - T_2)/\Delta T$, where T^* is the fluid temperature. Considering a Newtonian fluid and assuming that the flow satisfies the Boussinesq approximation, the governing equations can be written in dimensionless form as:

$$\nabla \cdot \mathbf{v} = 0 \tag{1}$$

$$\frac{\partial \mathbf{v}}{\partial t} + (\mathbf{v}\cdot\nabla)\mathbf{v} = -\nabla p + T\mathbf{j} + \left(\frac{Pr}{Ra_E}\right)^{\frac{1}{2}}\nabla^2\mathbf{v} - Ha^2\left(\frac{Pr}{Ra_E}\right)^{\frac{1}{2}} v\mathbf{j} \tag{2}$$

$$\frac{\partial T}{\partial t} + (\mathbf{v}\cdot\nabla)T = \left(\frac{1}{Pr\,Ra_E}\right)^{\frac{1}{2}}\nabla^2 T + \frac{Ra_I}{(Ra_E^3\,Pr)^{\frac{1}{2}}} \tag{3}$$

where $\mathbf{v}$ is the velocity vector, t is the time, p is the pressure, and $\mathbf{j}$ is the unit vector along the $+y$ axis.

No-slip boundary conditions are imposed at all boundaries,

$$\mathbf{v} = 0 \quad \text{on } x = 0, 1 \text{ and } y = 0, 1 \tag{4}$$

constant temperatures at the vertical walls,

$$T = 0 \text{ on } x = 0 \quad \text{and} \quad T = 1 \text{ on } x = 1 \tag{5}$$

and zero heat fluxes at the horizontal walls,

$$\partial T/\partial y = 0 \quad \text{on } y = 0, 1 \tag{6}$$

The effect of viscous dissipation and Joule heating on the present flow are neglected. These simplifications are almost universal for all MHD natural convection flows. A comprehensive justification for the latter can be found in Gelfgat and Bar-Yoseph [10].

For $Pr = 0.0321$ some selected values of Ra_E and various Ha, the numerical calculations are initialized from steady unicellular solutions for $S = 0$ and are continued by gradually increasing S up to 100. The gradual runs start from $S = 0.1$ using the solutions for $S = 0$ as initial conditions and continue for S^{new} $(=S^{old} + \Delta S)$ using solutions for S^{old} as initial conditions (typically, $\Delta S = 0.1S^{old}$).

Eqs. (1)–(3) together with the boundary conditions are solved by using a finite-volume technique based on the SIMPLE pressure–velocity coupling algorithm [15]. A second-order accurate implicit scheme is used for the transient terms, central discretization for the diffusion terms, and the modified QUICK scheme proposed by Hayase et al. [16] for the convection terms. The discretized equations are solved by using the SOR method. At each step, the solution is iterated until the normalized residuals of the mass, momentum and temperature equations become smaller than ϵ $(=10^{-5})$, which typically is reached in less than 50 iterations.

A nonuniform and staggered grid similar to the mesh distribution of Janssen et al. [17] was used. Special consideration for the number of grid points is given so that the narrow Hartmann boundary layers are adequately covered at the boundaries. A fruitful discussion for the thickness of Hartmann layers in buoyancy-driven convection could be found in Alboussière et al. [18]. The effect of spatial and temporal size increments on the flow and heat transfer characteristics have been examined for the higher values of the parameters considered in the present calculations. Grid independence tests showed that for the case $Ra_E = 10^6$, $Ha = 38$ and $S = 100$, a grid of 71×71 size results in less than 2% relative error of the maximum streamfunction and the average Nusselt numbers from the finer grid of 101×101 used. The time increment has been tested in the range of 0.0001–0.01. Considering the accuracy and the computational cost, a time step of $\Delta t = 0.002$ was used for the present calculations.

3. Numerical assessment

In a previous work [19] the present numerical method was compared successfully with the work of de Vahl Davis [20] for the steady-state flow of a laterally heated cavity. The unsteady hydrodynamic part of the present numerical method ($Ha = 0$) was tested also against the work of Shim and Hyun [8] for a laterally and volumetrically heated cavity. Due to a higher Prandtl number ($Pr = 0.7$) used in their work, only the initial transients and the final steady-state fields could be compared. The numerical solutions for $Ra_I = 0$ and various Ra_E were used as initial stages for the unsteady calculations. At $t = 0$, the internal heat sources were suddenly switched on. After several time steps the flow become again steady state. As Table 1 shows, the results of the present model are in very good agreement with those of Shim and Hyun [8].

The gradual numerical method which is adopted in the present study was essentially the same proposed by Wakitani [21] for the study of natural convection in a vertical cavity. The case for a cavity with aspect ratio (height/length) 20 for a fluid with $Pr = 0.71$ (air) was used for testing the numerical method. Starting from a steady single-cell flow pattern for $Ra = 10^3$, a five-cell pattern was observed for $Ra = 8 \times 10^3$, unsteady multicellular patterns for $2.3 \times 10^4 < Ra < 3.8 \times 10^4$, a steady single-cell flow pattern for $3.8 \times 10^4 < Ra < 1.3 \times 10^5$, steady five and four-cell patterns for $1.3 \times 10^5 < Ra < 4 \times 10^5$, and finally unsteady double-cell flow patterns were observed for $Ra > 4 \times 10^5$. Furthermore, the present method was capable to predict satisfactorily the frequencies and the amplitudes of the velocity and the temperature time evolution for the indicated case of $Ra = 2.6 \times 10^4$. Considering possible differences in the increments chosen for Ra, the gradual results of the present model are in good agreement with those of Wakitani [21].

The ability of the present numerical model to predict the onset of an oscillatory flow in laterally heated rectangular cavities under external magnetic fields was tested against the results of a stability analysis conducted by Gelfgat and Bar-Yoseph [10]. The aspect ratio (length/height) of the cavity was 4 and it was filled with a low Prandtl number fluid ($Pr = 0.015$). The case of a single-cell flow under the influence of a horizontal magnetic field was considered. Comparisons were based on three cases of critical Grashof numbers, 1.32×10^5, 5.37×10^6 and 5.50×10^6. The first two, for $Ha = 0$, correspond to steady-state solutions, while the third for $Ha = 20$ corresponds to an oscillatory flow. The results presented in Table 2 for the minimum and the maximum values of the streamfunction for the steady-state cases and the period of the oscillation ($\mathscr{T}$) for the unsteady case are in good agreement (relevant error less than 0.3% for a 140×70 mesh size) with those of Gelfgat and Bar-

Table 1
Comparison of the present method against Shim and Hyun [8]

	Ψ_{min}	T_{max}	Ψ_{min}	T_{max}	Ψ_{min}	T_{max}	Ψ_{min}	T_{max}
$Ra_E = 10^5$, $Ra_I = 10^6$	$t = 0$		$t = 0.01$		$t = 0.05$		$t = 0.1$	
Present	−13.72	0.5	−14.83	0.5	−16.79	0.748	−17.01	0.868
Shim and Hyun [8]	−13.7	0.5	−14.8	0.51	−16.8	0.75	−17.0	0.87
$Ra_E = 10^5$, $Ra_I = 10^7$	$t = 0.005$		$t = 0.008$		$t = 0.01$		$t = 0.02$	
Present	−17.13	1.048	−22.0	1.439	−24.05	1.708	−24.489	2.948
Shim and Hyun [8]	−17.1	1.05	−22.0	1.44	−24.0	1.71	−24.5	2.95

Table 2
Comparison of the present onset of oscillatory flow with Gelfgat and Bar-Yoseph [10]

	Gr_{cr}	Ha	Ψ_{min}	Ψ_{max}	$\mathscr{T}$
Gelfgat and Bar-Yoseph [10]	1.32×10^5	0	0.0	79.625	–
Present 80×40			0.0	79.226	–
Present 140×70			0.0	79.453	–
Gelfgat and Bar-Yoseph [10]	5.37×10^6	20	−1.919	365.18	–
Present 80×40			−2.738	262.85	–
Present 140×70			−2.002	364.16	–
Gelfgat and Bar-Yoseph [10]	5.50×10^6	20	–	–	3.3×10^{-3}
Present 80×40			–	–	2.51×10^{-3}
Present 140×70			–	–	3.3×10^{-3}

Yoseph [10]. In fact, they have used successfully a similar numerical method to validate their own results of a stability analysis, unfortunately without providing details about the grid size and time step used.

4. Results and discussion

4.1. Flow and temperature fields

Fig. 2 shows typical streamlines and isotherms for $Ra_E = 10^6$ and various values of Ha and S numbers. All these cases correspond to steady-state flow and are used to demonstrate the different flow patterns that could exist depending firstly on the imposed heating and secondly on the magnitude of the magnetic field. Fig. 2a corresponds to a unicellular flow pattern, as a result of the low S value of 5.5. Although internal heating is relative small in this case, its effect has started to be significant as illustrated by the isotherms. The internal heat added into the fluid has the tendency to increase the temperature of the upper fluid layers in the enclosure, a fact that also determines the shape of the streamlines. The bicellular flow pattern of Fig. 2b corresponds to a higher S value of 14.5. The temperature gradient between the hotter upper wall and the colder right sidewall is the reason for the formation of the second local circulation. The fluid temperature in the enclosure is higher than that of the sidewalls as a consequence of the increased internal heating. Acharya and Goldstein [6] showed that as the ratio S become higher than 10, the resulting temperature distribution is suitable for the formation of an almost similar intensity steady-state circulation pair at $S \approx 100$. Thus, the temperature of the mid-plane of the cavity is much higher than the temperature of the sidewalls. These flow patterns are extended on the whole right and left subdomains of the cavity, as in the case of the volumetrically heated square enclosure reported by Arcidiacono et al. [11] for $Gr = 10^5$. This phenomenon is rather impossible to appear in the present low Prandtl number fluid flow because of the increased convection (the corresponding Gr number for $Ra_E = 10^6$ is approximately 3×10^7). Fig. 2c shows a bicellular pattern with the same features as mentioned above that could be formed due to the strong magnetic field imposed (high Ha number). As the ratio S decreases, a third smaller cell appears at the bottom right corner of the cavity as a result of the temperature difference between the hot fluid layer and the colder wall. For higher S numbers, the lower circulation emerges with the upper one. The formation of the three-cell flow pattern is illustrated in Fig. 2d.

A general observation concerning the stability characteristics of all flow patterns shown in Fig. 2 can be made from their corresponding isotherms where areas of hot fluid layers below cold layers are observed. It is known from hydrodynamic stability theory (e.g. [22]) that when light fluid is below heavy fluid, the density distribution could lead to an instability and oscillations. This stability theory is also valid for the case when Lorentz forces are acting on the fluid body as discussed below.

Having as initial conditions the solution of a previous simulation with lower ratio S, the time evolution of the flow could be steady or unsteady depending on the stability characteristics of the flow at the increased ratio S. These two representative transition situations of the current flow are shown in Fig. 3 where the time evolution of the horizontal velocity and the temperature at $(x, y) = (0.2, 0.8)$ is presented. The onset of a time-periodic unsteady flow due to the growth of travelling wave disturbances for the case $Ra_E = 10^6$, $S = 14.42$ and

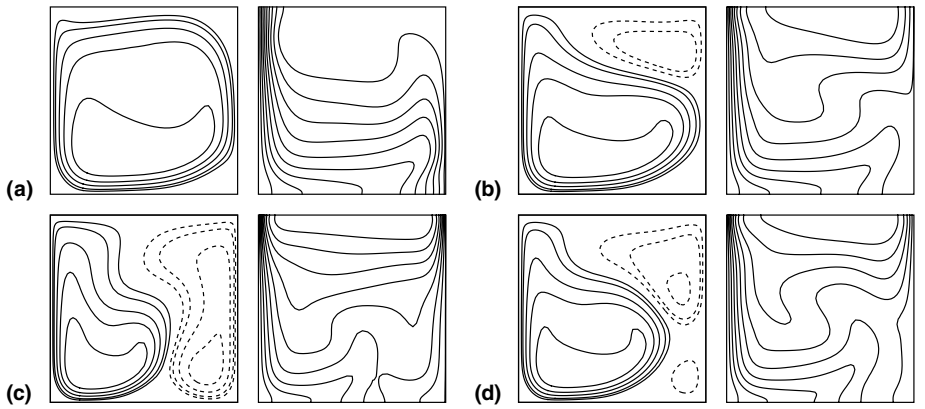

Fig. 2. Streamlines (left) and isotherms (right) for steady-state flow cases of $Ra_E = 10^6$: (a) unicellular flow pattern for $Ha = 38$, $S = 5.5$; (b) bicellular pattern for $Ha = 52$, $S = 14.5$; (c) bicellular pattern for $Ha = 76$, $S = 80.2$; (d) 3-cell pattern for $Ha = 52$, $S = 28.1$. All contour plots have been normalized with their maximum value. Constants of stream function are 0.8, 0.6, 0.4, 0.2, 0.1, −0.1, −0.2, −0.4 and −0.6, and the increment of the isotherms is 0.1.

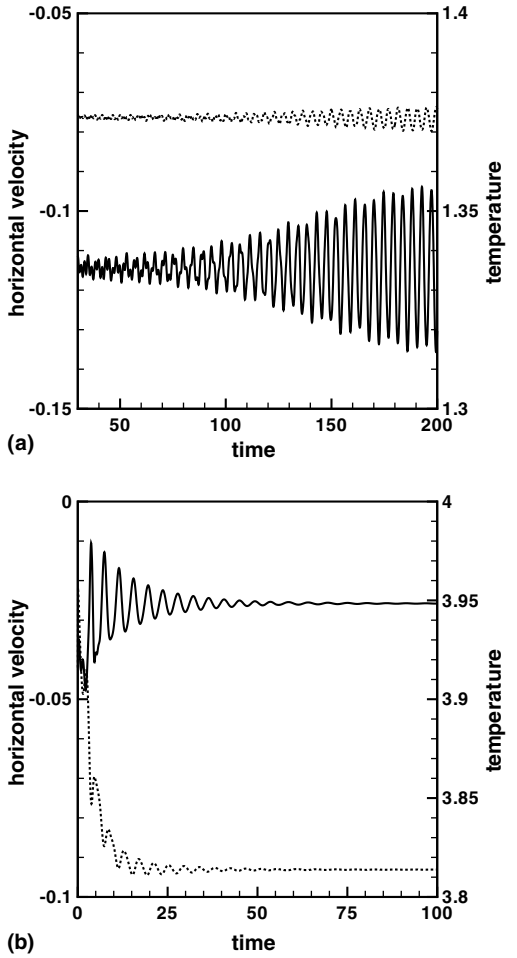

Fig. 3. Time evolution of horizontal velocity (solid line) and temperature (dashed line) at the location $(x, y) = (0.2, 0.8)$ for $Ra_E = 10^6$: (a) $S = 14.42$, $Ha = 40$; (b) $S = 80.17$, $Ha = 66$.

$Ha = 40$ is shown in Fig. 3a. This case corresponds to the transition from steady to unsteady bicellular flow for $t > 40$. The opposite situation of reverse transition from unsteady to steady bicellular flow pattern occurs at $t > 50$ for the case of $Ra_E = 10^6$, $S = 80.17$ and $Ha = 66$, as shown in Fig. 3b.

A complete picture of the flow patterns is shown in Fig. 4a and b for $Ra_E = 10^5$ and 10^6, respectively, and for the range of S and Ha numbers studied. These have been constructed from the 1500 unsteady flow cases mentioned earlier. For $Ra_E = 10^5$ and $S \leqslant 10$, a unicellular steady flow pattern is observed which is totally unaffected by the Hartmann number as shown in Fig. 4a. A similar conclusion can be drawn for the higher Ra_E case of Fig. 4b, for $S \leqslant 7$. Thus, the increase of Ra_E causes a shrink of the area occupied by the unicellular flow patterns. Moreover, all unicellular flow patterns for $Ra_E = 10^5$ studied here appear to be steady state, while for $Ra_E = 10^6$ and $Ha < 38$ the unicellular flow patterns are unsteady. Thus, the role of the magnetic field in the formation of the unicellular flow patterns is to determine their oscillatory features as Ra_E increases. On the other hand, the magnetic field has an increased influence on the oscillatory characteristics of 2-cell and 3-cell flow patterns. For $Ra_E = 10^5$, almost all the parameter area defined by $Ha < 4$ and $10 < S < 20$ is occupied by 3-cell steady and unsteady flow patterns. For the higher values of the ratio S, besides the dominant 3-cell flow structure, a number of smaller local cells could appear. The remaining parameter area is occupied by 2-cell flow patterns. In contrast, for $Ra_E = 10^6$, 3-cell steady and unsteady flow structures are extended for almost all the Ha numbers studied and confined in a very short range of S numbers. Thus, both Fig. 4a and b are in agreement with the main tendency of the present flow to form bicellular flow patterns as the ratio S increases. Moreover, it

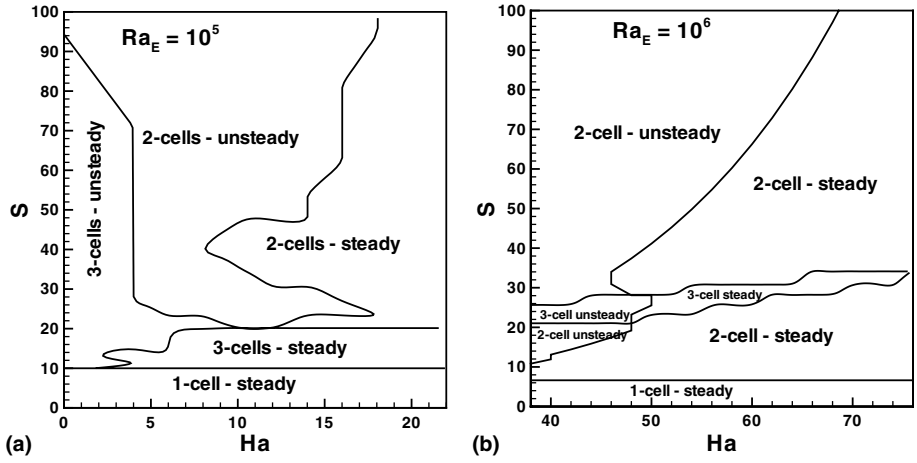

Fig. 4. Flow patterns and stability chart: (a) $Ra_E = 10^5$; (b) $Ra_E = 10^6$.

seems that, for $Ra_E = 10^6$, the higher the Ha number is, the higher the range of the S numbers required for the formation of the 3-cell structures.

The role of the ratio S and the magnetic field intensity on the flow stability is also clearly demonstrated in Fig. 4. The magnetic stabilization effect in buoyant convection flows has been the subject of many works, among others by Kaddeche et al. [23]. One could expect that the higher the Ha number, the higher the S number where steady flow patterns appear, although this statement is not quite accurate for the present case as illustrated in Fig. 4. In fact, for $Ra_E = 10^5$, there are two areas, in which the increase of Ha number with increasing S number leads from steady to unsteady flow, returns to steady flow as S increases and finally, for high S values, returns to unsteady flow patterns. The first small area is confined at $2 < Ha < 4$ and $10 < S < 15$ and corresponds to the region when the unicellular flow pattern changes to a 3-cell pattern. The second larger area is confined at $8 < Ha < 18$ and $20 < S < 40$ and is located near the region of the transformation of the 3-cell flow patterns to bicellular one. For $Ra_E = 10^6$, this phenomenon is less intense but still present and connected straightforward to the change of the flow patterns from 2-cell to 3-cell structures in the area of $Ha < 50$ and $10 < S < 30$.

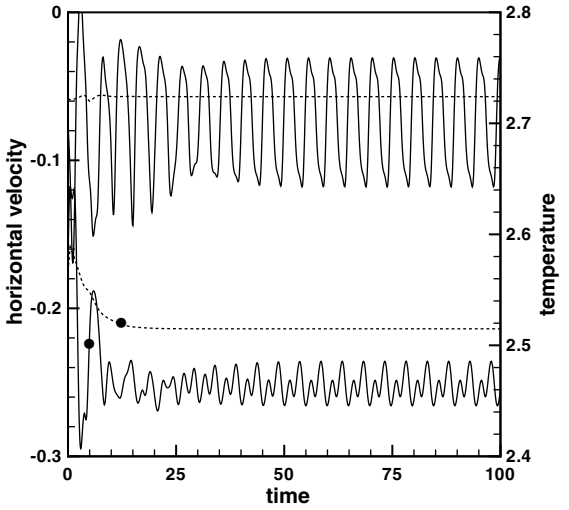

Fig. 5. Time evolution of horizontal velocity and temperature (marked with ●) at $(x, y) = (0.2, 0.8)$ for $Ra_E = 10^6$ and $S \simeq 41$: $Ha = 38$ (solid lines), $Ha = 76$ (dashed lines).

The results for the representative case of $Ra_E = 10^6$ and $S = 41.14$ at two Ha numbers (38 and 76) are selected to illustrate the effect of increasing magnetic intensity on the flow and temperature fields. As shown by the time evolution of the horizontal velocity and temperature in Fig. 5, the increase of the Hartmann number results primarily to the switch-off of the oscillations. The increase of the conduction heat transfer mode with increasing Ha, causes also a decrease of the fluid velocity at $(x, y) = (0.2, 0.8)$ and an increase of the temperature.

The shape of the flow and temperature fields is also affected by the increase of the Hartmann number as shown in Fig. 6. The time averaged isotherms of the unsteady case $Ra_E = 10^6$, $S = 41.14$ and $Ha = 38$ shown in Fig. 6a indicate that only in the core region of the left wider circulation cell hot fluid is below colder one which is a characteristic configuration for the initiation of flow unsteadiness. The increase of Ha number results in a more stratified temperature field which is unable to give oscillatory flow. For $S \gg 1$ and very intense magnetic

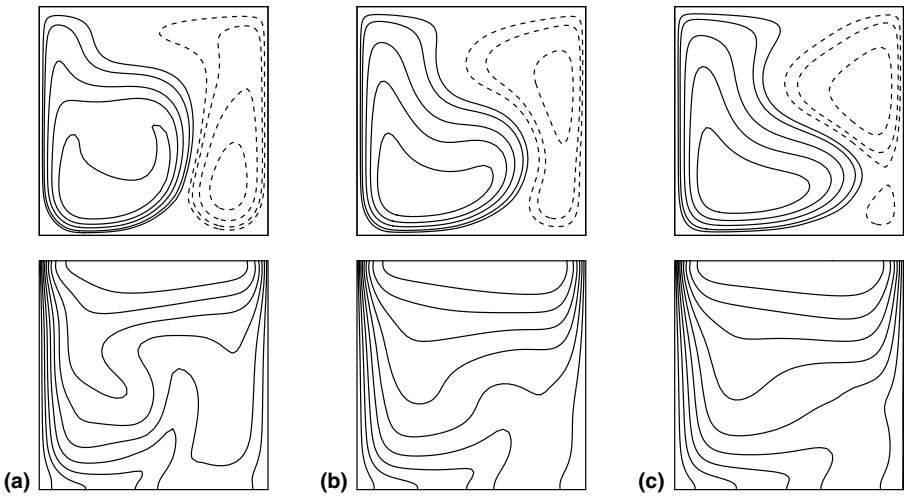

Fig. 6. Streamlines (top) and isotherms (bottom) for $Ra_E = 10^6$, $S \simeq 41$: (a) time averaged patterns for $Ha = 38$; (b) steady-state patterns for $Ha = 76$; (c) patterns for $Ha = 100$ (increments as in Fig. 2).

fields, one should expect the formation of an almost identical pair of flow circulations as a result of the near-symmetric temperature distribution with respect to the enclosure mid-plane. Similar flow patterns have been reported also for the lower convective cases of the volumetrically heated enclosures by Arcidiacono et al. [11]. In order to verify this hypothesis, in addition to the above two cases of $Ha = 38$ and 76, a special simulation was conducted for $Ha = 100$, taking as initial conditions the solution for $Ha = 76$. For the lower Ha value of 38, the time averaged recirculations of Fig. 6a extend in each side of the enclosure, with the left being wider, but close to a symmetric solution. In spite of our initial guess, as the Hartmann number increases, the right smaller circulation has the tendency to occupy a wider space at the upper layers of the enclosure, as shown in Fig. 6b for the steady-state case of $Ha = 76$ and in Fig. 6c for the case of $Ha = 100$.

For the above case of $Ha = 76$ (corresponding to a steady-state 2-cell flow) after some short initial transients, both velocity and temperature are stabilized due to the strong damping magnetic force. The opposite situation is observed for the case of $Ha = 38$, which corresponds to an unsteady 2-cell flow pattern. At about $t = 25$, the monitoring of the velocity and temperature indicates the onset of a transition to a time-periodic flow. Only one frequency for both quantities is present in this unsteady case. A detail of the periodic time evolution of the horizontal velocity and the temperature at $(x, y) = (0.2, 0.3)$ of the enclosure is shown in Fig. 7. The internal streamline plots correspond to characteristic locations in the period of the velocity time series. It appears also that the flow unsteadiness is caused mostly because of the fluid circulation of the left larger cell, rather than a complete rearrangement of the flow structure.

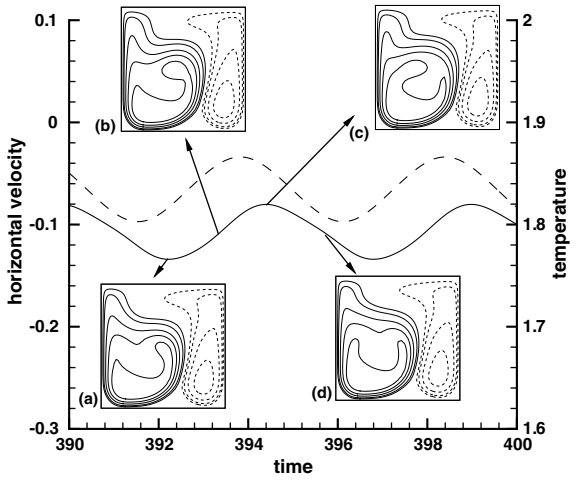

Fig. 7. Temporal variation of horizontal velocity (solid line) and temperature (dashed line) at $(x, y) = (0.2, 0.3)$ for $Ra_E = 10^6$, $S \approx 41$ and $Ha = 38$. Internal streamline plots at: (a) $t = 392.2$; (b) $t = 393.3$; (c) $t = 394.4$ and (d) $t = 396$ (increments as in Fig. 2).

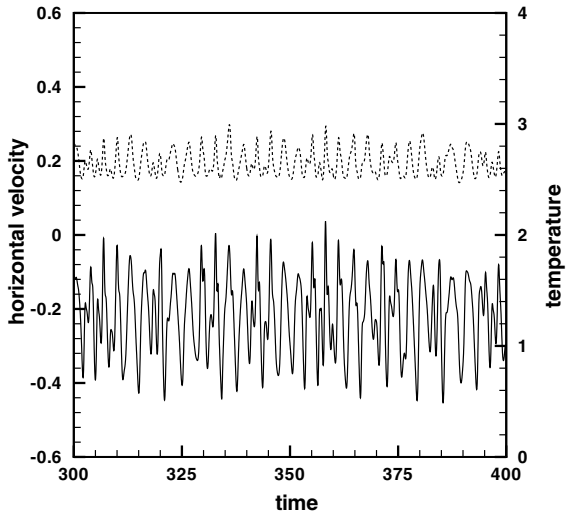

Fig. 8. Time evolution of horizontal velocity (solid line) and temperature (dashed line) at $(x, y) = (0.8, 0.3)$ for $Ra_E = 10^6$, $S = 100$ and $Ha = 38$.

The above case of single-frequency, time-periodic flow is not representative for all the oscillatory flow cases studied here. In fact, for a wide range of Ha and S numbers which result in unsteady flows, there appeared multi-frequency flow patterns. For high S and low Ha numbers, even chaotic flows are encountered, a result that has been reported also by Arcidiacono et al. [11] for $Gr > 10^8$. Such a chaotic case is well depicted in Fig. 8 for the case of $Ra_E = 10^6$, $S = 100$ and $Ha = 38$. This figure shows the irregular time evolution of the horizontal velocity and the temperature at the location $(x, y) = (0.8, 0.3)$.

In contrast to the time-periodic case of Fig. 7, in the present higher convective case of $S = 100$, both circulation cells shown in Fig. 9 are oscillatory. The isotherms show that the instability occurs at the center of each circulation cell mainly because hot fluid is below colder one due to the cold buoyancy plume which is formed at the middle of the cavity. In spite of the chaotic time evolution of the flow and temperature fields, the shape of the two main circulation cells remain almost unchanged, and no significant secondary cells are formed. Thus, the chaotic behavior of this flow is the result of the aperiodic motion of the fluid in the core regions of the cells. It seems that higher values of the S ratio are required for a complete rearrangement and formation of small and multiple circulation cells (a more familiar picture of chaotic flows).

It is interesting to examine the power spectral density of the above primitive-stage turbulent flow in order to

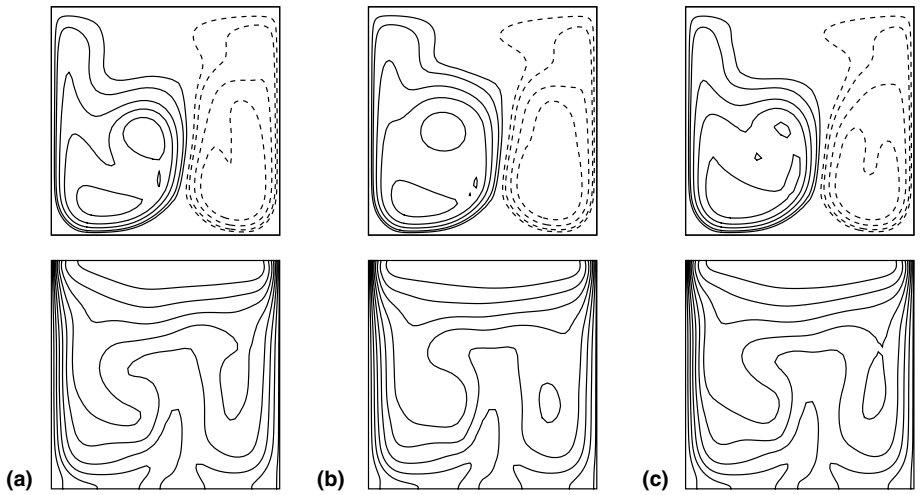

Fig. 9. Streamlines (top) and isotherms (bottom) for $Ra_E = 10^6$, $S = 100$, and $Ha = 38$: (a) $t = 390$; (b) $t = 395$; (c) $t = 400$. Contours normalized by maximum value. Increments as in Fig. 2.

compare it with the four regions of the power spectrum reported by Di Piazza and Ciofalo [24] for a volumetrically heated slender cavity with $Gr = 1.29 \times 10^9$. The power spectrum shown in Fig. 10 was calculated from the time evolution of the horizontal velocity at $(x, y) = (0.2, 0.8)$ from $t = 0$ to $t = 400$. An inspection of the spectrum shows that all four areas described in [24] are also present here. Thus, the first low-frequency region is formed for $f < 0.04$ where broad peaks appear. Unlike the spectrum of [24], for $0.04 < f < 0.3$ a region of significant power is formed with almost uniform distribution. Probably this region corresponds to the near-periodic oscillations of the outer layers of the main circulation structures. The second intermediate energy-containing region of [24] is also formed here in the narrow range of $0.3 < f < 0.5$. This region is characterized by a slope close to $-5/3$, predicted by Kolmogorov's theory of homogeneous turbulence. The third dissipation region of [24] is also formed for $0.5 < f < 3$ which is characterized by a decrease of the power content of the fluctuations. The slope of -6 encountered in this region is also predicted by [24]. The last region is a numerical tail due to the FFT algorithm and extends up to $f = 250$.

4.2. Heat transfer

The heat transfer characteristics of the present flow configuration are of technological importance, mainly because of the existence of the magnetic field. As Al-Najem et al. [25] showed, the increase of the Hartmann number causes reduction of the heat transfer rates from the cavity sidewalls. This phenomenon is related to the damping effect of the increasing magnetic field which

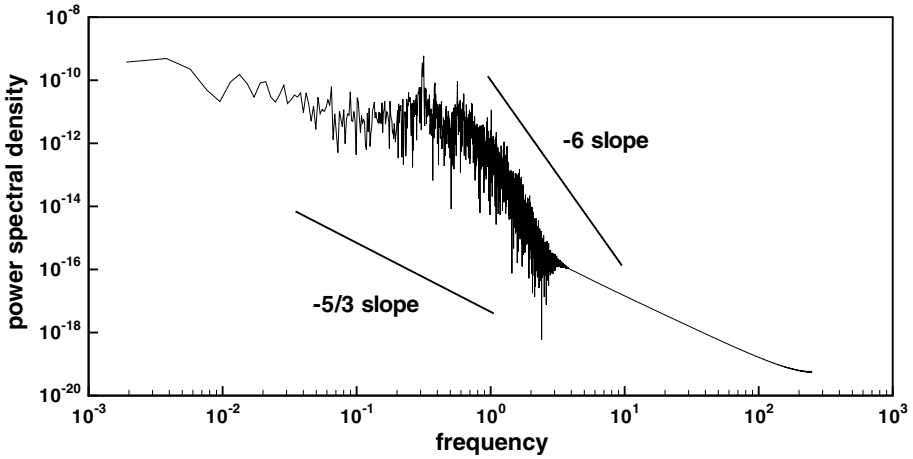

Fig. 10. Power spectrum of horizontal velocity at $(x, y) = (0.2, 0.8)$ for $Ra_E = 10^6$, $S = 100$ and $Ha = 38$.

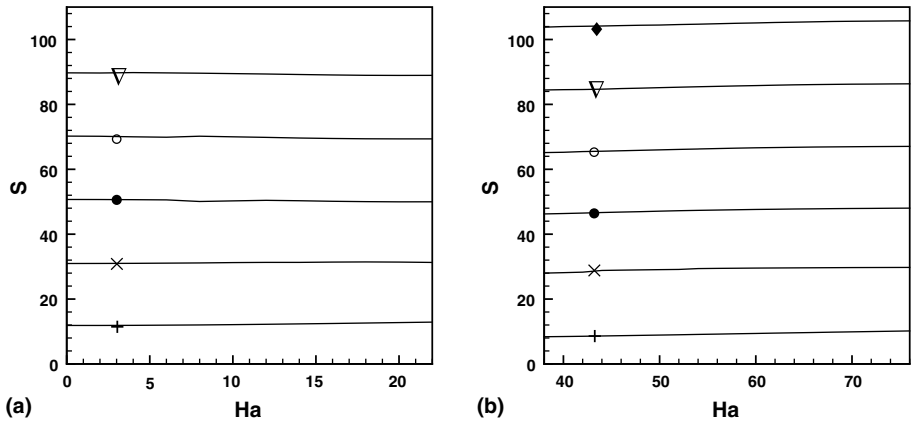

Fig. 11. Contours of the averaged Nusselt numbers at the cold sidewall (time averaged) on S–Ha space: (a) $Ra = 10^5$; (b) $Ra = 10^6$. Contours are marked: $\overline{Nu} = 10$ (+), 20 (×), 30 (●), 40 (○), 50 (▽), 60 (♦).

results in the domination of conduction over convection heat transfer. A measure of the heat transfer rates at the cavity walls is the average Nusselt number defined by Shim and Hyun [8] for the left wall as:

$$\overline{Nu} = \int_0^1 \left(\frac{\partial T}{\partial X}\right)_{X=0} \mathrm{d}Y \tag{7}$$

The values of the average Nusselt number at the left sidewall for the range of S and Ha numbers studied are presented in Fig. 11a and b for $Ra_E = 10^5$ and 10^6, respectively. For the unsteady flow cases, the corresponding Nusselt number has been time-averaged. The increase of S results in an increase of the heat transfer, as a consequence of the heat added internally. For the relatively small range of Hartmann numbers studied, no significant influence of the magnetic field on heat transfer could be discerned. As showed by Acharya and Goldstein [6], the overall energy balance in the cavity requires that:

$$\int_{Y=0}^{1} \left(-\frac{\partial T}{\partial X}\right)_{X=0} \mathrm{d}Y + \frac{Ra_I}{Ra_E} - \int_{Y=0}^{1} \left(-\frac{\partial T}{\partial X}\right)_{X=1} \mathrm{d}Y = 0 \tag{8}$$

The above criterion was satisfied in all the calculations presented here. Another reason for the insignificant influence of the magnetic field on the heat transfer is the low Prandtl number of liquid-metals used in this study. It is known that when $Pr \to 0$, the temperature appears to be only a function of the coordinates. Thus, the temperature distribution is controlled mainly by diffusion rather than convection heat transfer.

5. Conclusion

A numerical study of unsteady two-dimensional MHD natural convection of a liquid-metal in a laterally and volumetrically heated square cavity was presented. The range of parameters studied was from 10^5 to 10^6 for the external Rayleigh number, Ra_E, 0 to 100 for the ratio $S = Ra_I/Ra_E$, where Ra_I is the internal Rayleigh number and a range of Hartmann numbers, Ha, for which the flow for $S = 0$ was steady. The flow patterns appeared to be steady unicellular and multicellular or unsteady multicellular. For $Ra_E = 10^5$ and $S \leqslant 10$, and for $Ra_E = 10^6$ and $S \leqslant 7$, unicellular flow patterns occurred. For $Ra_E = 10^5$, the area defined by $Ha < 4$ and $10 < S < 20$ corresponded to 3-cell steady and unsteady flow patterns, while the remaining area to 2-cell flow patterns. For $Ra_E = 10^6$, 3-cell steady and unsteady flow structures were obtained for all Ha numbers studied and a narrow range of S numbers. The flow oscillations were reduced or vanished for increased Hartmann numbers due to the magnetic field damping effect, but not analogous to the increase of the ratio S. The heat transfer is enhanced with increasing S, but no significant effect of the magnetic field was observed due to the small range of the Hartmann numbers studied.

Acknowledgements

This work has been performed in the framework of the EURATOM—Hellenic Republic Association and is supported by the European Union within the Fusion Program. The content of this publication is the sole responsibility of the authors and it does not necessarily represent the views of the Commission or its services.

References

[1] N.B. Morley, S. Smolentsev, L. Barleon, I.R. Kirillov, M. Takahashi, Liquid magnetohydrodynamics—recent pro-

gress and future directions for fusion, Fus. Eng. Des. 51–52 (2000) 701–713.
[2] L. Barleon, U. Burr, K.-J. Mack, R. Stieglitz, Heat transfer in liquid metal cooled fusion blankets, Fus. Eng. Des. 51–52 (2000) 723–733.
[3] T. Tagawa, H. Ozoe, Enhancement of heat transfer rate by application of a static magnetic field during natural convection of a liquid metal in a cube, ASME J. Heat Transfer 119 (1997) 265–271.
[4] I.D. Piazza, M. Ciofalo, MHD free convection in a liquid-metal filled cubic enclosure—I. Differential heating, Int. J. Heat Mass Transfer 45 (2002) 1477–1492.
[5] I.D. Piazza, M. Ciofalo, MHD free convection in a liquid-metal filled cubic enclosure—II. Internal heating, Int. J. Heat Mass Transfer 45 (2002) 1493–1511.
[6] S. Acharya, R.J. Goldstein, Natural convection in an externally heated vertical or inclined square box containing internal energy sources, ASME J. Heat Transfer 107 (1985) 855–866.
[7] T. Fusegi, J.M. Hyun, K. Kuwahara, Natural convection in a differentially heated square cavity with internal heat generation, Numer. Heat Transfer 21 (1992) 215–229.
[8] Y.M. Shim, J.M. Hyun, Transient confined natural convection with internal heat generation, Int. J. Heat Fluid Flow 18 (1997) 328–333.
[9] A.Y. Gelfgat, P.Z. Bar-Yoseph, A.L. Yarin, On oscillatory instability of convective flows at low Prandtl number, ASME J. Fluids Eng. 119 (1997) 823–830.
[10] A.Y. Gelfgat, P.Z. Bar-Yoseph, The effect of an external magnetic field on oscillatory instability of convective flows in a rectangular cavity, Phys. Fluids 13 (8) (2001) 2269–2278.
[11] S. Archidiacono, I.D. Piazza, M. Ciofalo, Low-Prandtl number natural convection in volumetrically heated rectangular enclosures II. Square cavity, AR = 1, Int. J. Heat Mass Transfer 44 (2001) 537–550.
[12] P.A. Davidson, An Introduction to Magnetohydrodynamics, Cambridge University Press, Cambridge, 2001.
[13] J.P. Garandet, T. Alboussière, R. Moreau, Buoyancy driven convection in a rectangular enclosure with a transverse magnetic field, Int. J. Heat Mass Transfer 35 (4) (1992) 741–748.
[14] S. Ostrach, Natural convection in enclosures, ASME J. Heat Transfer 110 (1988) 1175–1190.
[15] S.V. Patankar, D.B. Spalding, A calculation procedure for heat, mass and momentum transfer in three-dimensional parabolic flows, Int. J. Heat Mass Transfer 15 (1972) 1787–1806.
[16] T. Hayase, J.A.C. Humphrey, R. Greif, A consistently formulated QUICK scheme for fast and stable convergence using finite-volume iterative calculation procedure, J. Comput. Phys. 98 (1992) 108–118.
[17] R.J.A. Janssen, R.A.W.M. Henkes, C.J. Hoogendoorn, Transition to time-periodicity of a natural-convection flow in a 3D differentially heated cavity, Int. J. Heat Mass Transfer 36 (1993) 2927–2940.
[18] T. Alboussière, J.P. Garandet, R. Moreau, Buoyancy-driven convection with a uniform magnetic field. Part 1. Asymptotic analysis, J. Fluid Mech. 253 (1993) 545–563.
[19] I.E. Sarris, I. Lekakis, N.S. Vlachos, Natural convection in rectangular tanks heated locally from below, Int. J. Heat Mass Transfer 47 (2004) 3185–3216.
[20] G. de Vahl Davis, Natural convection of air in a square cavity: A benchmark numerical solution, Int. J. Numer. Meth. Fluids 3 (1983) 249–264.
[21] S. Wakitani, Flow patterns of natural convection in an air-filled vertical cavity, Phys. Fluids 10 (8) (1998) 1924–1929.
[22] P.G. Drazin, W.H. Reid, Hydrodynamic Stability, Cambridge University Press, Cambridge, UK, 1981.
[23] S. Kaddeche, D. Henry, H.B. Hadid, Magnetic stabilization of the buoyant convection between infinite horizontal walls with a horizontal temperature gradient, J. Fluid Mech. 480 (2003) 185–216.
[24] I.D. Piazza, M. Ciofalo, Low-Prandtl number natural convection in volumetrically heated rectangular enclosures I. Slender cavity, AR = 4, Int. J. Heat Mass Transfer 43 (2000) 3027–3051.
[25] N.M. Al-Najem, K.M. Khanafer, M.M. El-Rafaee, Numerical study of laminar natural convection in tilted enclosure with transverse magnetic field, Int. J. Numer. Meth. Heat Fluid Flow 8 (1998) 651–672.